Retrieval methods of effective cloud cover for the GOME instrument: an intercomparison

O. N. E. Tuinder, R. de Winter-Sorkina, P. J. H. Builtjes

Atmos. Chem. Phys. Discuss., 2, 623–668, 2002
www.atmos-chem-phys.org/acpd/2/623/

Atmospheric Chemistry and Physics Discussions

Retrieval methods of effective cloud cover for the GOME instrument: an intercomparison

O. N. E. Tuinder[1], **R. de Winter-Sorkina**[1], **and P. J. H. Builtjes**[2]

[1]Institute for Marine and Atmospheric Research Utrecht (IMAU), Utrecht University, Utrecht, The Netherlands
[2]TNO MEP, Apeldoorn, the Netherlands

Received: 11 April 2002 – Accepted: 13 May 2002 – Published: 12 June 2002

Correspondence to: O. N. E. Tuinder (tuinder@phys.uu.nl)

Abstract

The radiative scattering by clouds leads to errors in the retrieval of column densities and concentration profiles of atmospheric trace gas species from satellites. Moreover, the presence of clouds changes the UV actinic flux and the photo-dissociation rates of various species significantly. The Global Ozone Monitoring Experiment (GOME) instrument on the ERS-2 satellite, principally designed to retrieve trace gases in the atmosphere is also capable of detecting clouds. Four cloud fraction retrieval methods for GOME data that have been developed are discussed in this paper (the Initial Cloud Fitting Algorithm, the PMD Cloud Retrieval Algorithm, the Optical Cloud Recognition Algorithm and the Fast Retrieval Scheme for Cloud Observables). Their results of cloud fraction retrieval are compared to each-other and also to synoptic surface observations. It is shown that all studied retrieval methods calculate an effective cloud fraction that is related to a cloud with a high optical thickness. Generally, we found ICFA to produce the lowest cloud fractions, followed by OCRA, then FRESCO and PC2K along four processed tracks (+2%, +10% and +15% compared to ICFA respectively). Synoptical surface observations gave the highest absolute cloud fraction when compared with individual PMD sub-pixels of roughly the same size.

1. Introduction

Modern satellites orbiting the Earth can provide users with a constant flow of data with a high spectral resolution and a full geographical coverage in a limited amount of time. From this data, it is possible to retrieve information about atmospheric constituents. The retrieval of density columns of trace gases such as O_3, NO_2, BrO, SO_2, OClO and HCHO and profiles of ozone, especially in the troposphere, are to some extent dependent on a correct description of the partially cloudy scenes in the field of view (Burrows et al., 1999; Hoogen et al., 1999; van der A et al., 1998; Munro et al., 1998; Koelemeijer and Stammes, 1999a). In radiative transfer calculations for retrieval, clouds are often

ACPD

2, 623–668, 2002

used as the reflecting lower boundary of the atmosphere and everything below may be parameterized as a ghost column or is not treated at all. Also, the calculation of photodissociation rates of many species in the atmosphere is influenced by the presence (or absence) of clouds. For example, scattering of light at a cloud layer can increase the diffuse backscattered radiation above this layer and at the same time shield the layers below from the strong direct component of sunlight, leading to significant differences in the actinic flux (van Weele and Duynkerke, 1993; Los et al., 1997).

The major factors in the reflection of light both above and under a cloud layer are, apart from the solar zenith angle, the micro- and macro-physical properties of the cloud itself like droplet radii, droplet number density, assymmetry factor, vertical extent and the height (indicated by either cloud top or cloud base).

As an illustration of the radiative transfer of two cases, a fully and partially clouded case, are shown in Fig. 1. Due to the scattering properties of the cloud and the cloud cover, the situation with a complete covered sky and a low optical thickness can give the same radiance at the Top Of the Atmosphere (TOA) as the situation where there is a partially cloud cover and a higher optical thickness. While the radiance at the TOA is almost the same, the vertical actinic flux profile (in a weighted plane parallel approach) is significantly different, leading to different local photolysis rates.

Satellites are better fit to produce regular cloud data with a global coverage for analysis of its distribution and trends than combining all surface observations alone. Since the beginning of use of meteorological and research satellites, a number of methods have been developed to retrieve the cloud fraction and other parameters of clouds. In this study we are using data from ESA's Global Ozone Monitoring Experiment (GOME). For GOME there has been one retrieval method in use for some time by the GOME Data Processor (GDP): the Initial Cloud Fraction Algorithm (ICFA) based on work by Kuze and Chance (1994). In recent years three other methods were developed: the PMD (Polarization Measurement Device) Cloud Retrieval Algorithm (PCRA) by Kurosu and Burrows (1997), Kurosu and Burrows (1998), Kurosu et al. (1999) and von Bargen et al. (2000), the Optical Cloud Recognition Algorithm (OCRA) by Loyola (1998)

ACPD
2, 623–668, 2002

and von Bargen et al. (2000)) and the Fast Retrieval Scheme for Cloud Observables (FRESCO) by Koelemeijer and Stammes (2001).

In this study we will evaluate the cloud retrieval algorithms of the four methods mentioned above in order to better understand the consequences of their assumptions in the retrieved cloud fractions. For this, we compare the results of the retrieval of the four methods and also compare them to data from synoptical surface weather stations. The PCRA and OCRA implementation used in this study is our own code based on the description of the algorithms in articles and reports, ICFA data is used from the Level-2 product and FRESCO data was obtained from the Dutch SCIAMACHY Data Center. The time period used in our study are the months of August of 1997, 1998 and 1999.

In Sect. 2 of this paper, the GOME instrument and the data that are used will be described, in Sect. 3 the various cloud fraction retrieval methods will be reviewed, and in Sect. 4 the results of the comparisons will be shown. Finally, Sect. 5 is for the conclusion of this work.

2. The GOME instrument

The GOME instrument on board of the European Space Agency's ERS-2 satellite was launched in April 1995. GOME is a nadir viewing across track scanning spectrometer measuring the reflectivity of the Earth with a spectral resolution of 0.2 - 0.4 nm between 240 and 790 nm and it has a spatial resolution of 320 × 40 km^2 per ground pixel. Three ground pixels are scanned in the forward movement of the scanning mirror (±30°) and one pixel in the backward movement. The same wide swath of one pixel is also seen by three broad band Polarization Measurement Detectors (PMDs) in the same instrument (see Table 1) with a higher spatial resolution of 20 × 40 km^2, thus dividing a wide ground pixel into 16 smaller sub-pixels as shown in Fig. 2. For this study we only use the ground pixels scanned in the forward direction, and the PMD sub-pixels of these wide ground pixels. The ERS-2 satellite has a sun-synchronous near-polar orbit with a local equator crossing time of 10:30 AM. The orbits of three sequential days cover the

ACPD
2, 623–668, 2002

whole Earth, making it possible to get global coverage from the GOME instrument.

3. Cloud fraction detection methods

3.1. Reflectance at the top of atmosphere

The upward radiation at the top of the atmosphere consists of backscattered light due to Rayleigh scattering from air molecules, Mie scattering from clouds and aerosols, and reflected light from the surface of the Earth in the field of view. The radiation is measured by the spectral detector-array of the GOME instrument and by the broadband PMDs. These measurements are converted to albedo values by dividing the measured earth-shine by the solar irradiance and correcting for the length of the optical light path through the atmosphere due to solar zenith angle θ_0 and the line of sight angle θ to the satellite:

$$\varrho(\lambda) = \frac{\pi I(\lambda)}{F_0(\lambda)\cos(\theta_0)\cos(\theta)} \quad (1)$$

where $\varrho(\lambda)$ is the albedo at wavelength λ (nm) for the detector array or $\lambda = R, G, B$ for the broadband PMD channels, $I(\lambda)$ is the upward radiance and $F_0(\lambda)$ the solar irradiance at the top of the atmosphere.

3.2. Initial Cloud Fitting Algorithm

The Initial Cloud Fitting Algorithm (ICFA), based on work by Kuze and Chance (1994) is used for the operational level-2 GOME data processor (DLR, 1994) and provides the standard GOME cloud fraction for most users.

The ICFA method is based on a chi-square minimisation of high resolution measurements between 758 – 778 nm, comprising of reflectances in the continuum and the O_2-A absorption band (around 760 nm), and radiative transfer calculations of a simulated cloud. The reflectivity of the wavelength region outside the O_2-A band is mainly

ACPD
2, 623–668, 2002

influenced by the cloud cover f_c, the optical thickness τ and the surface albedo α_s. The reflectivity inside the band depends mainly on the cloud top height and the cloud fraction. This can be seen from Fig. 3, which shows the reflectance measured by the GOME instrument near the O_2-A band: in the right panel of this figure the clouded situation has a less deep O_2 – A band compared to the clear sky cases, because the cloud is blocking the absorption of light by the oxygen molecules below the cloud. The difference between a land or sea surface does not matter significantly to the relative depth of the O_2-A band. Due to the large size of the pixel, the complete set of GOME measurements are dominated by partially clouded scenes.

A number of assumptions are made for the radiative transfer calculations of the simulated cloud. The cloud reflectances $R_{\text{sim}}(\lambda)$ are found by using a weighted plane-parallel approach that is proportional to the cloud fraction which distinguishes between the cloudy part $R_{\text{cloud}}(\lambda)$ with a constant optical depth and the clear part $R_{\text{clear}}(\lambda)$. The only absorbing gas species in the atmosphere in this wavelength region is O_2, and all Rayleigh and Mie scattering are approximated by an additional closure term $R_{\text{closure}}(\lambda)$. The ground surface acts as Lambertian reflector, and the cloud top is modelled with a bi-directional reflectance function. At the top of the atmosphere (TOA), the netto effect of an increasing cloud fraction or increasing cloud top height or increasing optical thickness is in some cases the same, so that these three cloud parameters can not be retrieved all at the same time from the depth of the O_2-A band alone. To overcome this, a fixed optical thickness is taken for all types of clouds ($\tau_{\text{cloud}} = 20$) and a climatological monthly mean cloud top height is used from the ISCCP database (Rossow and Garder, 1993).

The simulated cloud reflectances $R_{\text{sim}}(\lambda)$ is then written as:

$$R_{\text{sim}}(\lambda) = f_c \cdot R_{\text{cloud}}(\lambda) \; + \; (1 - f_c) \cdot R_{\text{ground}}(\lambda) \; + \; R_{\text{closure}}(\lambda) \tag{2}$$

where f_c is the cloud fraction and the other components are:

$$R_{\text{cloud}}(\lambda) = f_c \alpha(\mu, \mu_0) \int \Theta(\lambda - \lambda_0) T_\lambda(P_c, \mu, \mu_0) d\lambda \tag{3}$$

ACPD
2, 623–668, 2002

$$R_{\text{ground}}(\lambda) = (1 - f_c)\beta \int \Theta(\lambda - \lambda_0) T_\lambda(P_g, \mu, \mu_0) d\lambda \quad (4)$$

$$R_{\text{closure}}(\lambda) = \gamma\,(1 - \lambda/\lambda_0) \quad (5)$$

with μ_0 and μ the cosine of the solar zenith angle and the viewing zenith angle, λ is the integration wavelength (758–778 nm), λ_0 indicates some reference wavelength, $\Theta(\lambda - \lambda_0)$ the entrance slit function, $T_\lambda(P_c, \mu, \mu_0)$ the transmission function of the atmosphere between the reflecting surface and the satellite, P_g and P_c the ground and cloud top pressure, and finally there are three parameters used for the χ^2 minimisation in Eq. (6): $\alpha(\mu, \mu_0)$ (the cloud top reflectivity), β (the ground reflectivity) and γ (a free parameter).

$$\chi^2 = \sum_{i=1}^{N} \left[\frac{R_{\text{meas}}(\lambda_i) - R_{\text{sim}}(\lambda_i)}{\epsilon(\lambda_i)} \right]^2 \quad (6)$$

where $\epsilon(\lambda_i)$ denote the errors in the individual reflection measurements. The χ^2 minimisation uses a set of pre-computed transmittances from a line by line code using O_2-A band absorption data from HITRAN '96 (Rothman et al., 1998).

Because of the fixed optical thickness, the ICFA method produces an effective cloud fraction, i.e. a cloud fraction that corresponds to the radiances of a cloud with an optical thickness of $\tau = 20$ and a cloud fraction f_c.

3.3. PMD Cloud Retrieval Algorithm

The PMD Cloud Retrieval Algorithm (PCRA) was first developed by Kurosu and Burrows (1997), later extended with the Revised Cloud Fitting Algorithm (RFCA) by Kurosu et al. (1999), and after that modified (von Bargen et al., 2000). PCRA is capable of calculating the cloud fraction from GOME data and in combination with RFCA also the cloud top height and the optical thickness. We will only look at the cloud fraction part in this study.

ACPD
2, 623–668, 2002

Except for snow and ice surfaces, clouds generally have a higher reflectance than the Earth's surface in the visual spectral range. By looking at the radiances detected by the PMD's this can be used to distinguish between cloud and the surface if the reflectance of the surface is known.

A lookup table for each 0.5° × 0.5° grid box (covering the Earth surface) was generated by processing all PMD pixels over a period of time (typically one month) and storing the minimum and maximum albedo of each of the three wavelength bands $\lambda_j = R, G, B$ (see Table 1) and a combination Z which is the ratio of the radiances of $\lambda = R$ and $\lambda = G$. All PMD sub-pixels i located in the same grid-box at (x, y) are evaluated to find the local minimum and maximum:

$$\varrho_{\min}(x, y, \lambda_j) = \min\left(\varrho_i(x, y, \lambda_j)\right) \tag{7}$$

$$\varrho_{\max}(x, y, \lambda_j) = \max\left(\varrho_i(x, y, \lambda_j)\right) \tag{8}$$

for $i = 1 \ldots n$

$$\varrho_{\min}(x, y, Z) = \min\left(\frac{\varrho_i(x, y, R)}{\varrho_i(x, y, G)}\right) \tag{9}$$

$$\varrho_{\max}(x, y, Z) = \max\left(\frac{\varrho_i(x, y, R)}{\varrho_i(x, y, G)}\right) \tag{10}$$

where the reflection $\varrho(\lambda)$ is defined as in Eq. (1), and n is the total number of PMD sub-pixels in grid-box (x, y).

The minimum and the maximum albedo $\varrho_{\min,\max}(x, y, \lambda_j)$ of the PMDs, also called 'thresholds', represent a cloud free and a completely clouded situation respectively. Margins δ can be applied to the threshold values to account for different optical densities of clouds (maximum threshold), aerosol density and slightly changing surface reflectivity (minimum threshold).

When the albedo of a PMD sub-pixel is above a maximum value $\varrho_{\max}(x, y, \lambda_j) - \delta$ or below a minimum value $\varrho_{\min}(x, y, \lambda_j) + \delta$ the algorithm assigns these pixels a cloud fraction of $f_c = 1$ or $f_c = 0$, respectively. All pixels that have not been classified by

ACPD
2, 623–668, 2002

this method are interpolated linearly to a fractional cloud cover between minimum and maximum value (plus or minus the margin value):

$$f_v(\lambda) = \varrho_i(x,y,\lambda) - \big(1 + \delta_{\min}(\lambda)\big)\varrho_{\min}(x,y,\lambda) \tag{11}$$

and also in case of sea:

$$f_v(Z) = \varrho_i(x,y,Z) - \big(1 + \delta_{\min}(Z)\big)\varrho_{\min}(x,y,Z) \tag{12}$$

or also in case of land:

$$f_v(Z) = \big(1 - \delta_{\max}(Z)\big)\varrho_{\max}(x,y,Z) - \varrho_i(x,y,Z) \tag{13}$$

$$f_{\text{range}}(\lambda) = \big(1 - \delta_{\max}(\lambda)\big)\varrho_{\max}(x,y,\lambda) \; - \; \big(1 + \delta_{\min}(\lambda)\big)\varrho_{\min}(x,y,\lambda) \tag{14}$$

$$f_{\text{subpixel}}(\lambda) = f_v(\lambda)/f_{\text{range}}(\lambda) \tag{15}$$

$$f_{\text{subpixel}} = \frac{1}{4}\sum_{\lambda=R,G,B,Z} f_{\text{subpixel}}(\lambda) \tag{16}$$

$$f_{\text{GOMEpixel}} = \frac{1}{16}\sum_{k=1\cdots16} f_{\text{subpixel},k} \tag{17}$$

The way $f_v(Z)$ is calculated for land and sea differs because in cloud free situations over land more green than red light is reflected, and over seas this situation is reversed. The original PCRA uses a flow diagram (details in Kurosu and Burrows, 1997) for land and sea surface types determining the order of the wavelength bands on which tests are applied when calculating the cloud fraction f_c. The most recent revision of the PCRA method (hereafter called PC2K) requires *all* channels and the ratio (R,G,B,Z) to be above or below the thresholds for a sub-pixel to be classified as cloudy or cloud free and sub-pixels that have PMD values inside the thresholds corrected by the margins are interpolated linearly like Eq. (11) and following equations for all channels.

ACPD
2, 623–668, 2002

3.4. Optical Cloud Recognition Algorithm

OCRA stands for Optical Cloud Recognition Algorithm and was developed by Loyola (1998). The cloud cover fraction is calculated by comparing the individual PMD sub-pixel to the previously stored cloud free (CF) composite reflectance database. To get this cloud-free surface reflectance database OCRA, normalizes the albedo values calculated by Eq. (1) by dividing the red and green component by the sum of all three components:

$$r = \frac{\varrho(x, y, \lambda_R)}{\sum_{j=R,G,B} \varrho(x, y, \lambda_j)}, \qquad g = \frac{\varrho(x, y, \lambda_G)}{\sum_{j=R,G,B} \varrho(x, y, \lambda_j)} \tag{18}$$

These r and g components are in normalised 'rg-space'. From r and g a vector $\overrightarrow{rg}$ can be defined as the line between the origin $(0, 0)$ and (r, g) with length $\|rg\| = \sqrt{r^2 + g^2}$.

After normalization, the distance in rg-space between the white point $\overrightarrow{w}$, representing a white clouded pixel, and the individual PMD sub-pixel $\overrightarrow{rg}_i$ is calculated. The PMD albedos (R_i, G_i, B_i) of the pixel with the maximum distance to $\overrightarrow{w}$ are then stored in a database on a $0.5^\circ \times 0.5^\circ$ grid. The maximal distance between $\overrightarrow{w}$ and the individual sub-pixel $\overrightarrow{rg}_i$ at location (x, y) is given as in Eq. (19):

$$\|\overrightarrow{rg}_{CF}(x, y) - \overrightarrow{w}\| \geq \|\overrightarrow{rg}_i(x, y) - \overrightarrow{w}\| \quad \text{for i} = 1 \cdots \text{n} \tag{19}$$

where $\overrightarrow{rg}_{CF}$ is the cloud free situation and n the total number of PMD sub-pixels in grid-box (x, y) that were used to make the cloud free composite.

The definition of 'white' is an equal amount of radiation in all three wavelength bands (red, green and blue). From this definition it can be easily shown that 'white' in rg-space is $\overrightarrow{w} = (r_{\text{white}}, g_{\text{white}}) = (\frac{1}{3}, \frac{1}{3})$.

After the cloud free composite has been made, the calculation of the cloud fraction f_c of a GOME pixel is done by calculating the fractions of the individual PMD sub-pixels

ACPD
2, 623–668, 2002

i and then averaging over all 16 sub-pixels in a GOME pixel:

$$f_i(\lambda) = \max\left(0,\ S(\lambda)\left[\left(\varrho_i(x,y,\lambda) - \varrho_{CF}(x,y,\lambda)\right)^2 - O(\lambda)\right]\right) \quad (20)$$

for λ = R,G,B

$$f_{c,i} = \sqrt{\sum_{\lambda=R,G,B} F_i(\lambda)} \quad (21)$$

$$f_c = \frac{1}{16} \sum_{i=1\cdots16} \min(F_{c,i}, 1.0) \quad (22)$$

where $S(\lambda)$ is a scaling factor and $O(\lambda)$ is an offset. Both $S(\lambda)$ and $O(\lambda)$ are empirical factors based on a comparison with other data. ICFA data was used to find a set of offset and scaling factors (Table 2): the offsets were found optimising clear sky pixels around $f_c = 0.0$ and the scaling factors were found optimising the median of the cloud cover frequency diagram using completely clouded pixels around $f_c = 1.0$. It should be noted that the offset and scaling factors in von Bargen et al. (2000) are considerably different from the values in table 2. This may be caused by the different dataset or methods used for the optimisation of these factors.

The scaling factors effectively define the cloud that is represented by OCRA: a lower $S(\lambda)$ lowers the cloud fractions, thus representing all clouds with a higher effective optical thickness and a higher $S(\lambda)$ does the opposite. The offset factors $O(\lambda)$ function as an additional threshold to account for aerosols and other effects unrelated to clouds that can increase the radiation.

The OCRA method has been implemented in the development version of the GOME Level 1-to-2 Data Processor and may be used as the default cloud fraction value in the future (von Bargen et al., 2000).

ACPD
2, 623–668, 2002

3.5. Fast Retrieval Scheme for Cloud Observables

The Fast Retrieval Scheme for Cloud Observables (FRESCO) developed by Koelemeijer and Stammes (2001) is capable of calculating cloud fractions and the cloud top height. It uses the radiances in wavelength regions of 1 nm wide inside and outside the O_2 A band: at 758 nm where there is no absorption, at 761 nm where there is strong absorption and at 765 nm where the absorption is moderate. A number of assumptions are made: absorption by gases occurs only by O_2 above clouds or the ground surface, scattering processes by air molecules and aerosols are neglected inside and below the cloud, and both the surface and the cloud top are assumed to be Lambertian reflectors. A simulation of the reflectance R_{sim} at the top of the atmosphere consists of a clear part with surface albedo A_s and a clouded part with the cloud albedo A_c (the weighted plane-parallel approach):

$$R_{\text{sim}} = (1 - f_c)\, T(\lambda, p_s, \theta, \theta_0)\, A_s + f_c\, T(\lambda, p_c, \theta, \theta_0)\, A_c \tag{23}$$

where f_c is the cloud fraction, T the transmittance, λ the wavelength, p_s and p_c are the surface and cloud top pressure, θ and θ_0 are the line of sight and solar zenith angles respectively. The absorption is calculated using HITRAN'96 data and a mid-latitude summer atmosphere (Anderson et al., 1986). The surface albedo is taken from a minimum reflectance database on a $2.5^\circ \times 2.5^\circ$ grid from GOME data itself using all data in the months of January and July, the sea surface albedo is taken as 0.02, and the cloud albedo is taken as 0.8. A non-linear least-squares minimisation is used to derive the cloud fraction and the cloud top pressure. For this minimisation the Levenberg-Marquardt method is used (Press et al., 1986).

The assumption of a fixed cloud albedo means that FRESCO works with an effective cloud fraction for clouds with an albedo of 0.8. This corresponds with a cloud with an optical thickness τ of about 50 for a solar zenith angle $\theta_0 = 0^\circ$ or smaller values for τ for increasing solar zenith angles (Los et al., 1997).

The difference between FRESCO en ICFA (which also uses wavelengths around the O_2 A band) is that FRESCO determines the effective cloud fraction and the cloud top

ACPD
2, 623–668, 2002

pressure at the same time, where ICFA determines only the effective cloud fraction.

3.6. Synoptic surface observations

Synoptic surface observations are taken at most operational weather stations and provide a cloud fraction in octas (steps of $\frac{1}{8}$) and the type of the most dominant cloud. Zero octas corresponds to a clear sky and eight octas corresponds to a completely covered sky. These synoptic observations are estimated to be representative for an area with a radius of 20 to 30 km (Rossow et al., 1993, and references therein) which corresponds roughly with the size of one PMD sub-pixel of $20 \times 40\,\mathrm{km}^2$.

In the comparison of surface observations with satellite based retrieval methods the location of the surface station has to be co-located with the (sub-)pixel. Also, as an additional requirement, the satellite over-pass must be within 30 minutes on either side of the moment of observation at the surface station. If the wind is blowing with a speed of $10\,\mathrm{ms}^{-1}$ parallel to the scan direction of the mirror (often east-west direction), all the clouds in one PMD pixel have moved to the adjacent PMD pixel in only 30 min.

In most cases, only one surface station is co-located within the area of one PMD sub-pixel which may lead to errors if the time difference is large or if the station is located at the border of the PMD pixel.

The cloud classification used comes from the so called $8N_sCh_sh_s$ indicator (or sometimes $8N_hC_LC_MC_H$) used in SYNOP weather reports, where '8' is the group-indicator, N_s indicates the cloud cover fraction of the most dominant cloud type C_s described in Table 3.

3.7. Possible problems with above methods

3.7.1. ICFA

ICFA uses the ISCCP monthly mean cloud top height database, which is a climatology based on measurements of clouds from satellites (MeteoSat, GMS, GOES and NOAA)

between July 1983 and June 1991 (Rossow and Garder, 1993). Although the monthly mean of cloud parameters in a grid-box may be reasonable accurate, it is likely that there is a difference between the actual cloud top height at the moment of retrieval at a location and the climatology. A comparison between ATSR-2 and ICFA effective cloud fractions have shown a mean difference of 18% with a standard deviation of 23% (Koelemeijer and Stammes, 1999b).

3.7.2. PCRA

The threshold databases are supposed to have attained their minimum and maximum values within a limited period of data. The vegetation and land use is seasonal dependent, restricting the period of data used for a minimum reflectance database to a month or a season at the most.

The assumption that the minimum values have been reached may not be valid for all locations on Earth, especially in the tropics near the Inter Tropical Convergence Zone and in other regions with a persistent cloud cover like the North Atlantic and North Pacific storm tracks.

PCRA has physically defined minima (clear sky thresholds) and maxima (totally covered with clouds) when the databases are created from sufficient data. One month is a good start for a $0.5^{\circ} \times 0.5^{\circ}$ grid database, three months is more than sufficient for the mid-latitudes and shows some unusual areas of low reflectance ('black spots') in the minimum database that may eventually lead to incorrect results (although the minimum reflectance is less important than a well established maximum).

An effect of using data from a long period is that the maximum thresholds are likely to become higher and the minima lower: the thresholds are taking more extreme values. This means a shift towards the retrieval of optically thick clouds as they have a higher reflectance than thin clouds, which will lead to a bad description of the absolute cloud fraction of optically thin clouds.

ACPD
2, 623–668, 2002

3.7.3. OCRA

The method OCRA uses to arrive at a cloud free reflection database is based on getting the point furthest away from 'white' in normalised rg-space, aiming to reach a value that will be cloud free which also has the lowest reflection. The normalization method uses the ratio of the reflections measured by the PMD channels and has lost information about the absolute value of the reflection itself. This normalization and search mechanism does not guarantee that the saved PMD values are indeed cloud free and correspond to the lowest reflectance available, although this minimum reflectance is required in the cloud fraction calculation phase.

Visual inspection of the cloud free database of OCRA (made with this 'furthest from white' method) shows a 'patchy' surface, while PCRA minimum thresholds provides a more smooth image of the Earth. An example of this is shown in Fig. 4. These minimum threshold images were made using one month of data in August, but also three-year composites of August months show the same patchy behaviour from grid point to grid point in OCRA and did not seem to improve to the level of smoothness of a one-month PCRA minimum threshold image. This means that part of the calculated pixel-to-pixel differences in OCRA are likely to come from different minima than from real cloud features.

The OCRA algorithm is not independent of other retrieval algorithms because the scaling and offset factors are optimised to reach a good agreement with an other data source (in this case ICFA).

3.7.4. FRESCO

The clear sky surface albedo database has grid cells with a size of $2.5^{\circ} \times 2.5^{\circ}$. Surface characteristics may differ considerably within such a large area which may increase the uncertainty in areas of mixed surface type (e.g. coasts, mixed agricultural and urban areas). Also, the spectrometer of GOME is known to be degrading and the spectral characteristics of the clear sky database may change over time. This can also

be a point of concern for the ICFA method but not for PCRA and OCRA which use a threshold database that is restricted in time.

3.7.5. SYNOP

One of the problems of comparing SYNOP surface measurements to satellite derived measurements is that, while looking at the same cloud, the determined cloud fraction may be different. Part of this difference may be explained by taking into account the distance of the cloud layer to the observer and the path through which it is observed: for the human observer on the ground the cloud is at a few hundred meter or a few kilometer in altitude, seen through the hazy boundary layer which limits the observer to about 20 to 30 kilometer radius, while the satellite instrument observes the same cloud from above at 800 km altitude through mostly optically thin air. An other issue is the definition of a cloud: a human observer may define a cloud as the portion of the sky that is 'white' on a blue-ish background, while the satellite instrument is using calibrated spectral radiances or broadband measurements. Cloud fractions reported in the SYNOP reports are classified by the eye of humans and, although trained for this work and following standards set by the WMO, the results may differ per individual. A satellite instrument stays the same, and should give similar results in similar cases in all parts of the world (when degradation of the instrument is not taken into account). Cloud fractions reported by surface observers are supposed to be independent of the cloud optical thickness but geometrical effects with clouds with a larger vertical structure may increase the reported cloud cover.

3.8. Data sources

The data we used for this paper is from the months of August 1997, 1998 and 1999 in which a number of GOME pixels located near the Netherlands were selected (Fig. 5). The clear sky composites for PCRA and OCRA were made for each of the three years using all PMD data in August of that particular year. The ICFA values are taken from

ACPD
2, 623–668, 2002

the most recent revision of the level-2 data (R02) and the FRESCO data comes from the Dutch SCIAMACHY Data Center. The synoptic surface observations used in the comparisons are from weather stations within the Netherlands and some observations from ships on the North-Sea that were collected at 10:00, 11:00, and 12:00 UTC.

4. Results

4.1. Comparison for different types of clouds.

In Sect. 3.2 and 3.5 we have seen that ICFA and FRESCO use a fixed optical thicknesses τ of 20 and about 50, respectively, in their calculations of the cloud fraction, independent of the type of cloud. For PCRA/PC2K and OCRA the cloud fraction is determined by the threshold database and the offset and scaling factors, also independent of the type of cloud. A human observer however, can both estimate the cloud fraction and classify types of clouds with different optical thicknesses.

To study the effect that different types of clouds can have on the retrieved cloud fraction, we separate the clouds by class of optical thickness (Table 4).

Figure 6 shows the comparison of PC2K cloud fractions with surface observations for co-located sub-pixels which are separated by cloud type (top) and the frequency analysis of the cloud fractions respectively (bottom).

The anti-correlation in the histogram panel on the left shows that clouds with a low optical thickness and a large fractional cover are represented by the algorithm as a thick cloud with a small cloud fraction. The centre plot shows that clouds with a medium optical thickness are also represented by a cloud with a smaller fractional cover than observed from the surface, although the anti-correlation is less strong. The number of data points with thick clouds is, regrettably, very small.

The reducing anti-correlation of the clouds with a low to medium optical thicknesses is in accordance with the expected smaller amount of radiation from these clouds with the same cloud cover compared to optically thick clouds which reflect much more

ACPD
2, 623–668, 2002

light to the satellite instrument. Since PC2K interpolates the cloud fractions between the minimum and the maximum value in the threshold database, cloud fractions of clouds with a low optical thickness are scaled to a thick effective cloud. A similar anti-correlation was found in a comparison with OCRA.

It must be noted that for PC2K the effective cloud fraction scaling only takes effect if the maximum threshold was created with sufficient data to ensure a complete cloud cover to be stored in the database. The effective cloud fraction scaling of OCRA is determined by the scaling factors.

This leads to the conclusion that all current available retrieval methods for a cloud fraction from GOME data, either using the O_2 A band or the PMDs, scale the cloud fraction to that of an effective optically thick cloud. This has a significant effect on the local actinic flux in the troposphere and thus also on photolysis rates (Tuinder et al., accepted by JGR, 2002).

4.2. Comparison of the retrieval methods and SYNOP with ICFA

The ICFA cloud fraction is at this moment the standard retrieved cloud fraction from the operational GOME level-2 data product and therefore, first the comparison between ICFA and the other retrieval methods will be presented. Also the comparison between ICFA and SYNOP surface measurements will be shown.

In Fig. 7 the comparisons between the cloud fractions averaged over all PMD sub-pixels in a GOME pixel are shown against ICFA for the four different retrieval methods. The error bars on the ICFA values are the uncertainties according to the level-2 data product. A margin of 5% was applied to the absolute values of the top and bottom PCRA thresholds for PMD channels $\lambda = R, G$ and B, and a margin of 0% was taken for the ratio Z. The margin for Z is set to zero because the effect on the selection of cloud fractions of $f_c = 0$ and $f_c = 1$ is very much influenced by Z due to its higher absolute value (on average $0.6 \leq Z \leq 1.1$) and corresponding larger margins of the minimum and maximum thresholds compared to the margins of regular PMD channels (on average $0.02 \leq \lambda = R, G, B \leq 0.27$). A PMD pixel would more likely be in the

ACPD
2, 623–668, 2002

margin zone of Z than the other channels and this would cause an unnatural shift to $f_c = 0$ or $f_c = 1$ if the margin for Z was taken 5% as well.

For the comparison between PC2K and ICFA, a margin of 5% was applied to all thresholds for PMD channels $\lambda = R, G$ and B and for the ratio Z as well (in contrast to the earlier PCRA method).

A comparison between averaged co-located SYNOP surface cloud fractions and the ICFA cloud fraction is shown in Fig. 8.

Table 5 contains the statistics of the plots in Figs. 7 and 8. Positive values of the mean difference indicate that the first mentioned method gives larger values. The table shows that the ICFA cloud fraction method generally gives lower values than the other retrieval methods (from 5% to 17% lower) and the surface observations (39% lower). Koelemeijer and Stammes (1999b) have indicated that ICFA also gives lower cloud fractions than the monthly mean ISCCP values. The overestimation of ISCCP was attributed to the threshold methods used to select between clear sky and (partly or fully) clouded pixels. Since partially clouded pixels would be classified as completely clouded, ISCCP is biased towards higher cloud fractions.

A visual comparison of the PCRA and PC2K plots in Fig. 7 gives the impression that both cloud fractions averaged over a GOME pixel behave very similar. This is confirmed by the statistics: both methods produce generally larger values than ICFA with the mean differences and other statistical parameters close to each other. The modification from PCRA to PC2K has changed the algorithm, but apparently has no significant impact on the results. This leads to the conclusion that both methods are interchangeable and for the following comparisons we will skip the older PCRA method and only present PC2K results.

The OCRA cloud fraction has the lowest mean difference and RMS and a standard deviation comparable to PC2K and FRESCO. The small mean difference and RMS are because the offset and scaling factors in Table 2 were determined using ICFA measurements, so this should not be surprising.

The mean differences of the retrieval methods are within the 20% error margin that

ACPD
2, 623–668, 2002

is often applied to ICFA values and estimated to be the difference between ICFA and an effective cloud fraction calculated from data from the ATSR-2 instrument on board ERS-2, having a spatial resolution of $1 \times 1\,km^2$ (Koelemeijer and Stammes, 1999b). An other study (von Bargen et al., 2000) reports an RMS error of 35.3% in a comparison between ICFA and ATSR-2.

The generally larger cloud fraction of each of the other retrieval methods compared to ICFA may be due to different causes. PCRA/PC2K uses a maximum threshold database which represents a complete cloud cover at each $0.5^0 \times 0.5^0$ gridbox, but there is no precise information on the optical thickness or the type of cloud that provided this maximum reflectivity. When the effective optical thickness of the maximum cloud cover is less than $\tau_{ICFA} = 20$, cloud fractions from the PCRA method will be larger than ICFA for the same situations. The slightly larger values from OCRA indicate that the scaling factors found also result in an effective cloud fraction that is less than τ_{ICFA}. A set of scaling factors with higher values will reduce the mean difference but not necessarily the RMS. Finally, the reason for the general larger cloud fractions from FRESCO is that it fits cloud fraction and cloud top height at the same time while using a cloud with an effective optical thickness around $\tau_{FRESCO} = 30 \sim 50$. A comparison of the cloud top height provided with ICFA and the value calculated by FRESCO shows that the cloud top height retrieved by FRESCO is generally lower than the value ICFA uses from the ISCCP database. A lower cloud top height gives a lower reflectivity and the cloud fraction needs to increase to compensate to get the same radiation at the top of the atmosphere.

The comparison of averaged co-located SYNOP ground observations with ICFA indicates that the cloud fraction reported by the surface observer is in most cases much larger than the cloud fraction of ICFA: the mean difference is 39%. The large difference between the averaged observations and the ICFA cloud fraction may be caused by a number of factors. The number of surface observations in a GOME pixel is generally small (2–6) compared to the number of PMD sub-pixels within a GOME pixel (16). If one takes into account the area for which the surface observation is representative (ra-

ACPD
2, 623–668, 2002

dius 20–30 km) and compares this to the size of the GOME pixel (320 × 40 km^2), the overlap between the GOME pixel and the represented areas by the surface stations is often not sufficient. The estimate the observer makes of the cloud cover may have been influenced by the geometry of the cover, especially in cases of broken clouds, where visible vertical sides of a cloud contribute to the covered area in the field of view.

4.3. Comparison of the methods against SYNOP surface observations using pixels near the Netherlands

The left panels of Fig. 9 show the comparisons between cloud fractions of individual PMD sub-pixels using PC2K and OCRA (top and centre), and FRESCO (bottom) versus the co-located individual SYNOP surface observations (cases 'ind. co-locations' in Table 6). For this comparison, the representative area of a PMD pixel and a synoptical observation is the same for PC2K and OCRA. The available PMD/SYNOP co-locations averaged over a GOME pixel is shown in the right panels (cases 'avg. co-locations'). The last type of cases in Table 6 is 'avg. over GOME pixel' where the average of all 16 PMD sub-pixels are compared against all available co-located SYNOP observations, so here also the PMD pixels without a co-located synoptical observation were taken into account. The values of the individual SYNOP observations on the vertical axis are fixed to 'strata' of multiples of octas (= $\frac{1}{8}$ of the hemisphere), where zero octa ($\frac{0}{8}$) is a clear sky and eight octa ($\frac{8}{8}$) means completely covered. Averaging, on the right, wipes the stratification as all co-located observations within a GOME pixel are taken into account.

The comparison of individual surface observations and individual satellite derived cloud fractions indicate that the surface observations overestimate the cloud algorithms in most cases where a surface cloud fraction of more than two octas is observed. Also, the plots show that the algorithms have difficulty getting a reasonable agreement with surface observations for higher observed cloud covers ($0.4 \leq f_c \leq 1.0$) where the range of solutions is wide. This can also be deduced from the statistics of these plots,

ACPD
2, 623–668, 2002

in Table 6 where we find mean differences of 20% – 38%, RMS of 27% – 44% and standard deviations of 18% – 24%. Averaging over all PMD sub-pixels and all co-located surface observations in a GOME pixel does not change the mean difference significantly. While the comparison between individual co-located surface observations and the FRESCO value is given, the averaged observation comparison gives a better indication because an individual sub-pixel is not representative for the whole GOME pixel.

The overestimation of surface observations compared to satellite measurements has also been noted in the ISCCP study by Rossow et al. (1993), where they did a comparison between 3 h global satellite cloud fraction data and over 670 000 surface observations and found an average overestimation of 11% and a standard deviation of 40%. This difference was reported to be seasonal dependent.

A comparison of PC2K and OCRA with high spatial resolution ATSR-2 cloud fractions (von Bargen et al., 2000) gave RMS errors of 27.5 and 27.1, respectively, which is lower than our comparison against SYNOP observations.

4.4. Comparison of data over a track

In this section we will compare the different cloud fraction detection methods along four tracks to study the consistency of the results for the same cases over a wider range of surface areas and cloud situations.

The ICFA cloud fraction of the central pixels of tracks with the data filename prefix 70802101, 70802114, 70802132 and 70802151 from 2 August 1997 are shown in Fig. 10. Figure 11 contains the cloud fractions by ICFA, PC2K, OCRA and FRESCO along the tracks. The mean cloud fraction and the standard deviation are given in Table 7 as a total over all 4 tracks.

Table 7 shows that the cloud fractions produced by ICFA are generally the lowest, followed by OCRA (+2%), then FRESCO (+10%) and PCRA (+15%). Although the behavior along the tracks are more or less the same, there are a few regions of special interest.

ACPD
2, 623–668, 2002

– Between 20N – 10N, track 70802101 shows that FRESCO indicates a cloud fraction $f_c = \pm 0.3$ where all the other methods indicate none. The soil surface along this part of the track is dry Sahara desert, and the sand may give a higher reflection than the surface database is correcting for, thus leading to a residue signal and interpreted it as a cloud fraction.

– At several areas along the tracks the ICFA cloud fraction is much lower than the cloud fraction of PCRA, OCRA or FRESCO. For instance around 50N and between 7S – 25S along track 70802101, between 60N and 20N along track 70802114, between 65N - 55N and 20S – 30S along track 70802132 and between 10S and 20S along track 70802151. A possible reason for this difference may be an incorrect cloud top height (taken from the climatology database) as most of these tracks-pieces are sea pixels which have a relatively low surface reflection.

In Table 8 the numerical mean difference, the RMS and the standard deviation of the difference of the various methods are given. We note again that the optimisation of the offset and scaling factors of OCRA works again to give a low mean difference but the RMS is comparable to the other ICFA cases. FRESCO and PC2K show a small mean difference, RMS and standard deviation, which may be caused by the similarity of the used methods: interpolation between clear sky minima from a grid and a fixed maximum or grid maximum, both with radiance characteristics of a thick cloud.

5. Conclusions

We have described the capabilities of the ICFA, PCRA/PC2K, OCRA and FRESCO cloud fraction retrieval methods for GOME. For this purpose we intercompared the retrieved cloud fractions of these methods together with co-located synoptical surface observations over the Netherlands for August 1997, 1998 and 1999.

ACPD
2, 623–668, 2002

A separation of clouds by optical thickness showed that clouds with a small optical thickness and a large fractional cover are represented by the retrieval methods as thick clouds with a small cloud fraction. This indicates that all four methods retrieve the cloud fraction as coming from a cloud with an effective high optical thickness. This can also be the reason for the wide spread of solutions for retrieved cloud fractions compared to surface observations with a cloud fraction $f_c > 0.4$.

In general, we found that ICFA produces the lowest cloud fractions, followed by OCRA, then FRESCO and PC2K along four processed tracks (+2%, +10% and +15% compared to ICFA respectively). Synoptical surface observations gave the highest absolute cloud fraction when compared with individual PMD sub-pixels of roughly the same size.

Concerning the OCRA method, the authors think that the method to find the Cloud Free database by normalization of the radiances producing an unnatural patchy behavior, and the necessity of determining the scaling and offset factors from other datasets make OCRA less suitable to be the standard cloud fraction product in the next generation of GOME data processors. PC2K or FRESCO may be better candidates for this purpose.

Acknowledgements. The authors wish to thank ESA for providing the GOME data, the Dutch SCIAMACHY Data Center for making the FRESCO data available, NWO/SRON for their financial support of this project and colleagues for their support preparing this paper.

References

Anderson, G., Clough, S., Kneizys, F., Chetwynd, J., and Shettle, E.: AFGL atmospheric constituent profiles, Tech. Rep. AFGL-TR-86-0110, Air Force Geophys.Lab., 1986. 634

Burrows, J., Weber, M., Buchwitz, M., Rozanov, V., Ladstädter-Weissenmayer, A., Richter, A., de Beek, R., Hoogen, R., Bramstedt, K., Eichmann, K.-U., Eisinger, M., and Perner, D.: The Global Ozone Monitoring Experiment (GOME): Mission concept and first scientific results, J. Atmos. Sci., 56, 151–175, 1999. 624

DLR: GOME level 1 to 2 algorithms description, Tech. rep., German Aerospace Center DLR, (Deutsches Zentrum fuer Luft- und Raumfahrt), 1994. 627

Hoogen, R., Rozanov, V., and Burrows, J.: Ozone profiles from GOME satellite data: algorithm description and first validation, J. Geophys. Res., 104, 8263–8280, 1999. 624

Koelemeijer, R. and Stammes, P.: Effects of Clouds on Ozone Column Retrieval from GOME UV Measurements, J. Geophys. Res., 104, 8281–8294, 1999a. 624

Koelemeijer, R. and Stammes, P.: Validation of GOME Cloud Fraction Relevant for Accurate Ozone Column Retrieval, J. Geophys. Res., 104, 18 801–18 814, 1999b. 636, 641, 642

Koelemeijer, R. and Stammes, P.: A fast method for retrieval of cloud parameters using oxygen A-band measurements from the Global Ozone Monitoring Experiment, J. Geophys. Res., 106, 3475–3490, 2001. 626, 634

Kurosu, T. and Burrows, J.: PMD Cloud Detection Algorithm for the GOME Instrument; Algorithm Description and Users-Manual; Draft version, Tech. rep., Institute of Remote Sensing, University of Bremen, 1997. 625, 629, 631

Kurosu, T. and Burrows, J.: PMD Cloud Detection Algorithm for the GOME Instrument; Algorithm Description and Users-Manual, Technical Report 11572/95/NL/CN, Institute of Remote Sensing, University of Bremen, European Space Agency, ESA/ESTEC, Noordwijk, The Netherlands. Annex to the ESA CADAPA Report, 1998. 625

Kurosu, T., Chance, K., and Spurr, R.: CRAG – Cloud Retrieval Algorithm for the European Space Agency's Global Ozone Monitoring Experiment, in: European Symposium on Atmospheric Measurements from Space, ESAMS '99, WWP-161, vol. 2, pp. 513–521, 1999. 625, 629

Kuze, A. and Chance, K.: Analysis of Cloud top height and cloud coverage from satellites using the O_2 A and B bands, J. Geophys. Res., 99, 14 481–14 491, 1994. 625, 627

Los, A., van Weele, M., and Duynkerke, P.: Actinic Fluxes in Broken Cloud Fields, J. Geophys. Res., 102, 4257–4266, 1997. 625, 634

Loyola, D.: A New Cloud Recognition Algorithm for Optical Sensors, IEEE International Geoscience and Remote Sensing Symposium, IGARSS'98 Digest Volume II, 572–574, 1998. 625, 632

Munro, R., Siddans, R., Reburn, W., and Kerridge, B.: Direct measurement of tropospheric ozone distributions from space, Nature, 392, 168–171, 1998. 624

Press, W., Flannery, B., Teukolsky, S., and Vetterling, W.: Numerical Recipes, Cambridge University Press, Cambridge, 1986. 634

Rossow, W. and Garder, L.: Cloud detection using satellite measurements of infrared and visible radiances for ISCCP, J. Climate, 6, 2341–2369, 1993. 628, 636

Rossow, W., Walker, A., and Garder, L.: Comparison of ISCCP and Other Cloud Amounts, J. Climate, 6, 2394–2428, 1993. 635, 644

Rothman, L., Rinsland, C., Goldman, A., Massie, S., Edwards, D., Flaud, J.-M., Perrin, A., Camy-Peyret, C., Dana, V., Mandin, J.-Y., Schroeder, J., McCann, A., Gamache, R., Wattson, R., Yoshino, K., Chance, K., Jucks, K., Brown, L., Nemtchinov, V., and Varanasi, P.: The HITRAN Molecular Spectroscopic Database and HAWKS (HITRAN Atmospheric Workstation): 1996 Edition, J. Quant. Spectros. Radiat. Transfer, 60, 665–710, 1998. 629

Tuinder, O., de Winter Sorkina, R., and Builtjes, P.: Impact of satellite derived effective cloud fraction on calculated actinic flux, photo-dissociation rates and OH production, J. Geophys. Res., accepted, 2002. 640

van der A, R., van Oss, R., and Kelder, H.: Ozone profile retrieval from GOME data, in: Remote Sensing of Clouds and the Atmosphere III, Proceedings of SPIE, (Ed) Russell, J., vol. 3495, pp. 221–229, 1998. 624

van Weele, M. and Duynkerke, P.: Effects of clouds on the photodissociation of NO_2: Observations and modelling, J. Atmos. Chem., 16, 231–255, 1993. 625

von Bargen, A., Kurosu, T., Chance, K., Loyola, D., Aberle, B., and Spurr, R.: ERS-2, Cloud Retrieval Algorithm for GOME (CRAG), Final Report, Tech. rep., German Aerospace Center (DLR) and Smithsonian Astrophysical Observatory (SAO), 2000. 625, 626, 629, 633, 642, 644, 652

Table 1. Spectral range of the Polarization Measurement Detector (PMD) channels

PMD nr	Spectral range [nm]	Associated color
PMD 1	295 – 397	Blue
PMD 2	397 – 580	Green
PMD 3	580 – 745	Red

ACPD
2, 623–668, 2002

Table 2. The OCRA scaling factors $S(\lambda)$ and offset factors $O(\lambda)$ per PMD channel used in this study

PMD nr (λ)	$S(\lambda)$	$O(\lambda)$
PMD 1 (blue)	17.0	0.0004
PMD 2 (green)	8.1	0.0004
PMD 3 (red)	6.9	0.0004

ACPD
2, 623–668, 2002

Table 3. Cloud classification C from the $8N_sCh_sh_s$ SYNOP code group

Nr	Type	Nr	Type
0	Cirrus (Ci)	5	Nimbostratus (Ns)
1	Cirrocumulus (Cc)	6	Stratocumulus (Sc)
2	Cirrostratus (Cs)	7	Stratus (St)
3	Altostratus (As)	8	Cumulus (Cu)
4	Altocumulus (Ac)	9	Cumulonimbus (Cb)

ACPD
2, 623–668, 2002

Table 4. Clouds divided by class of optical thickness (after von Bargen et al., 2000)

Optical Thickness	τ	Cloud Types
low	0 – 3.6	Cu, Ac, Ci, Cc
medium	3.6 – 23	Sc, As, Cs
high	23 <	St, Ns, Cb

ACPD
2, 623–668, 2002

Table 5. The mean difference (md) in %, the root-mean-square (RMS) in %, the standard deviation (sd) in %, the correlation coefficient (r^2) and the number of cases (N) of the comparison between ICFA and other retrieval methods and SYNOP surface observations, taken over all three years

Comparison	md	RMS	sd	r^2	N
PCRA – ICFA	13.9	21.7	16.7	0.501	281
PC2K – ICFA	14.1	21.5	16.3	0.510	281
OCRA – ICFA	4.6	18.5	17.9	0.502	281
FRESCO – ICFA	17.1	24.4	17.4	0.464	281
SYNOP – ICFA	38.9	44.2	21.0	0.467	234

ACPD
2, 623–668, 2002

Table 6. The mean difference (md) in %, the root-mean-square (RMS) in %, the standard deviation (sd) in %, the correlation coefficient (r^2) and the number of cases (N) of the comparison between SYNOP and retrieved cloud fraction methods, taken over all three years. Case description in the text

Comparison	md	RMS	sd	r^2	N
ICFA – SYNOP	−38.9	44.2	21.0	0.467	234
PC2K – SYNOP					
ind. co-locations	−25.3	33.7	22.1	0.469	662
avg. co-locations	−24.4	30.6	18.3	0.596	234
avg. GOME pixel	−22.9	29.3	18.1	0.603	234
OCRA – SYNOP					
ind. co-locations	−33.7	41.5	24.1	0.462	662
avg. co-locations	−32.7	38.3	19.9	0.576	234
avg. GOME pixel	−31.9	36.8	18.3	0.607	234
FRESCO – SYNOP					
ind. co-locations	−20.2	29.1	21.0	0.496	662
avg. GOME pixel	−19.7	27.5	19.1	0.559	234

ACPD
2, 623–668, 2002

Table 7.
Mean cloud fraction (mean) in %, the absolute difference (diff) to ICFA in %, the standard deviation (sd) in % and the number of pixels (N) of the comparison along the four tracks

Case	mean	diff	sd	N
ICFA	24.1	–	26.3	1845
PC2K	39.2	15.1	22.7	1845
OCRA	26.1	2.0	22.7	1845
FRESCO	34.2	9.5	24.7	1725

Table 8. Mean difference (md) in %, RMS in %, the standard deviation (sd) in % and the number of pixels (N) of the comparison along the tracks

Case	mean	RMS	sd	N
ICFA – PC2K	−15.1	26.9	22.2	1845
ICFA – OCRA	− 2.0	22.1	21.0	1845
ICFA – FRESCO	−9.5	22.7	20.6	1725
FRESCO – PC2K	−4.2	11.6	10.8	1725
FRESCO – OCRA	8.4	11.5	7.9	1725
PC2K – OCRA	13.1	16.6	10.1	1845

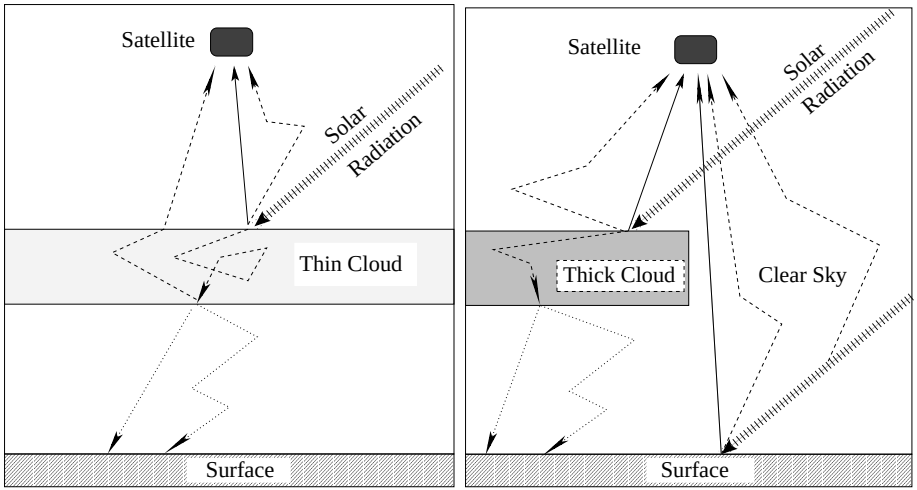

Fig. 1. Radiative transfer in a case where the optical thickness is low combined with a complete cloud cover (left) and a case where the optical thickness is high with a partially covered sky (right).

ACPD
2, 623–668, 2002

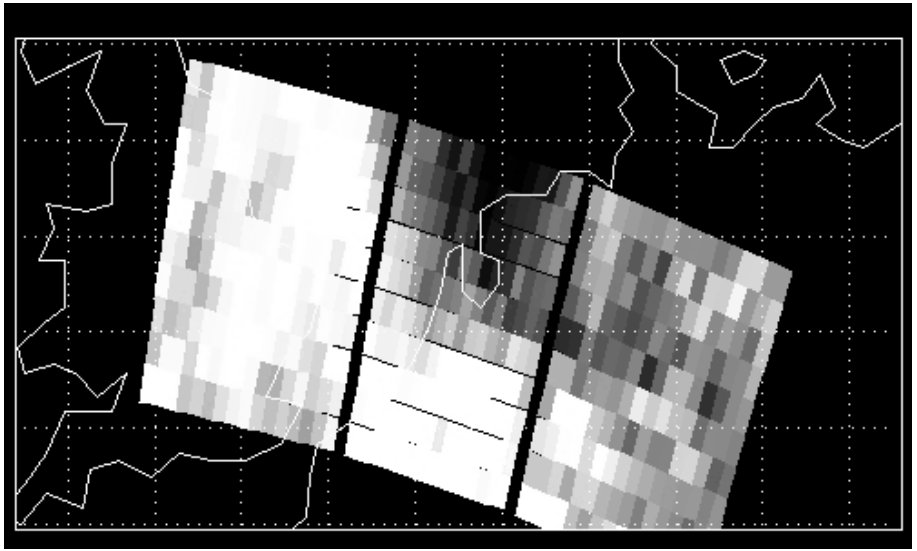

Fig. 2. Image showing the reflectance in 16 PMD sub-pixels inside each of a number of GOME pixels over the Netherlands (August 1st 1997, pixel nrs: 480 – 510 (north to south), tracknr 104).

ACPD

2, 623–668, 2002

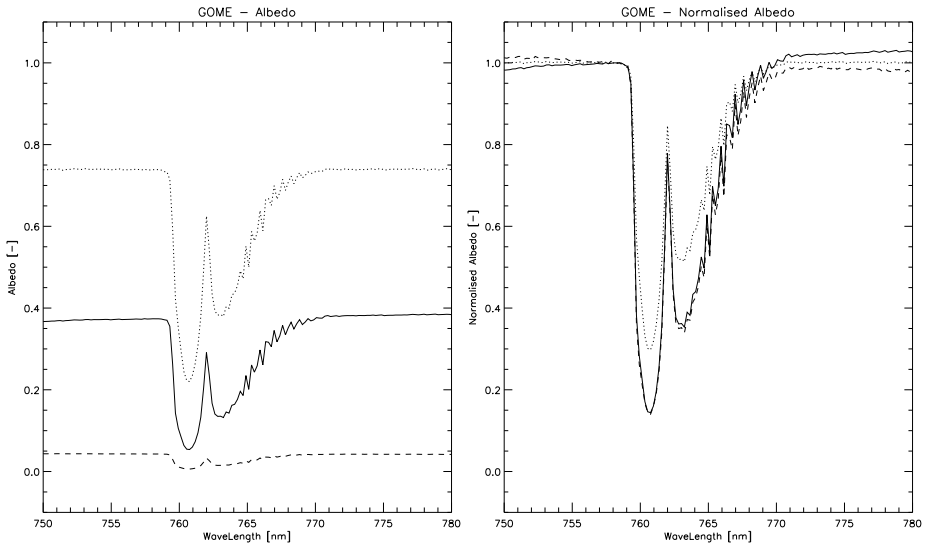

Fig. 3. Left: Reflectance measured by GOME near the O_2-A absorption band. The dotted line is a fully clouded scene, the solid line is a clear sky situation over land (the Netherlands), the dashed line is a clear sky situation over sea (the Atlantic Ocean). Right: Normalised albedo of the same situations (normalization wavelength λ_n = 758.0 nm).

ACPD
2, 623–668, 2002

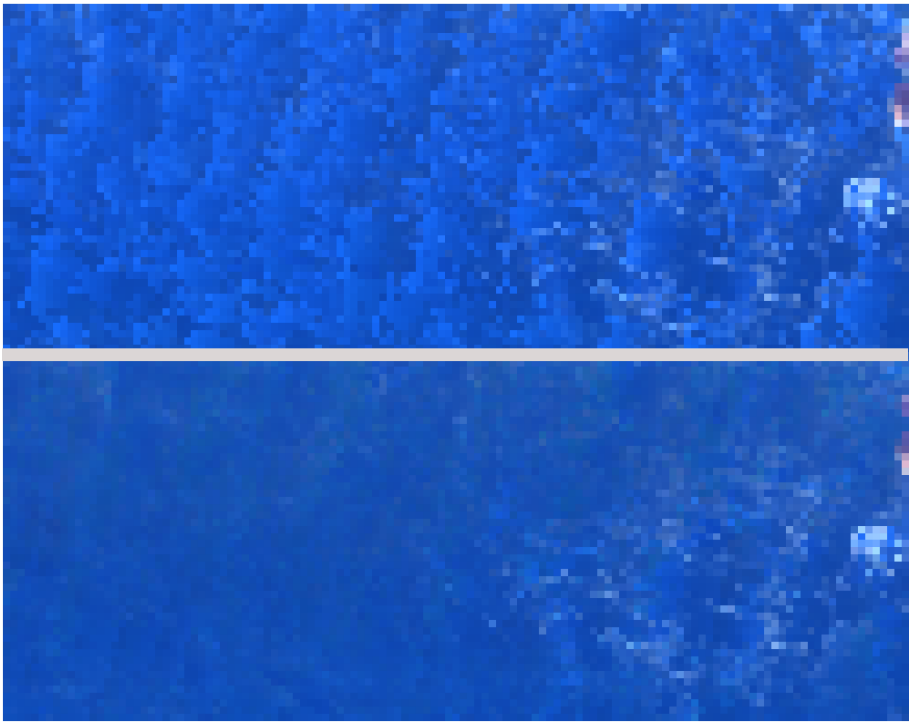

Fig. 4. An RGB image of the minimum reflectance surface databases of an area between 0S – 25S and 145W – 80W (Pacific Ocean) for OCRA (top) and PCRA (bottom).

ACPD
2, 623–668, 2002

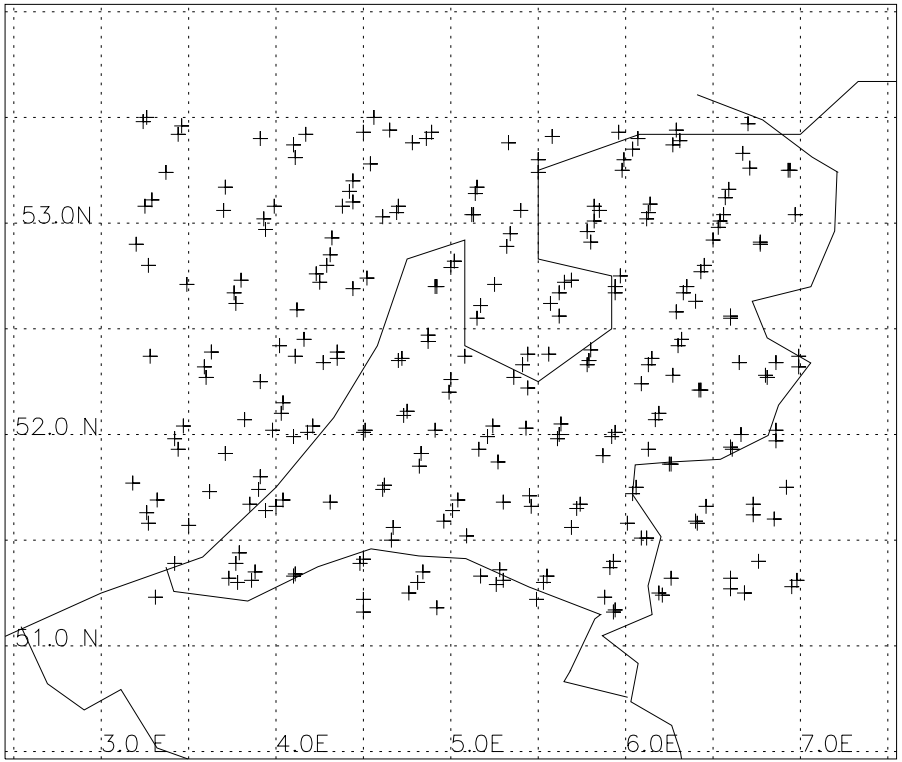

Fig. 5. Position of the centre of the GOME pixels above the Netherlands used in this section for the months of August 1997 (87 pixels), August 1998 (92 pixels) and August 1999 (102 pixels).

ACPD
2, 623–668, 2002

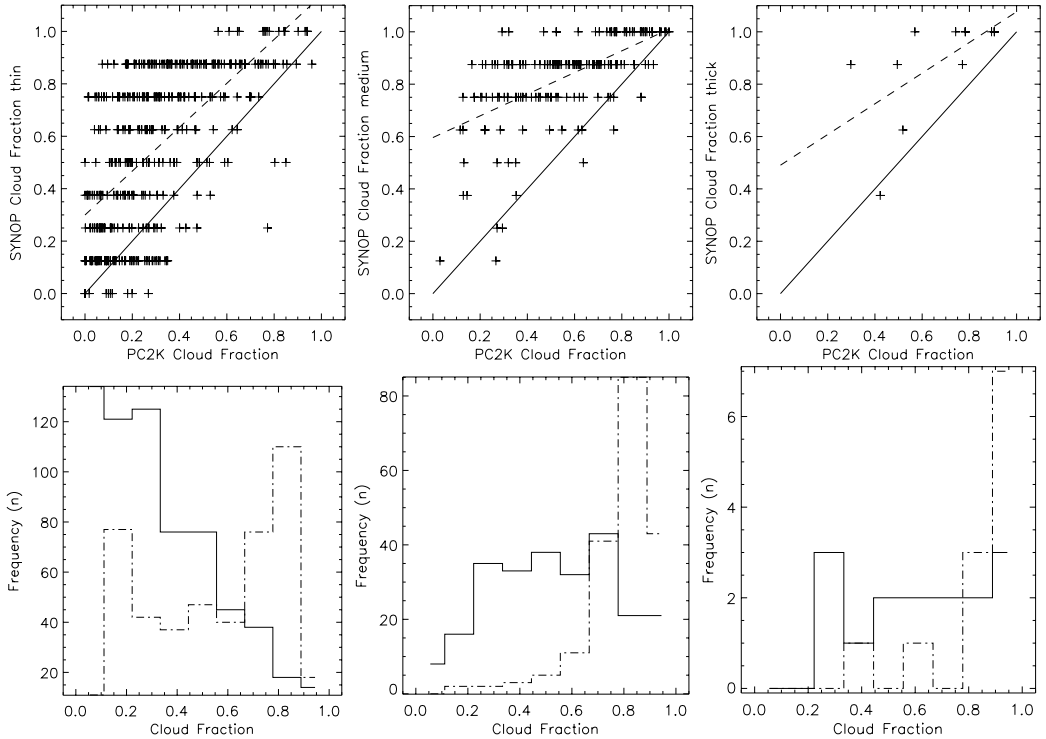

Fig. 6. Top: Individual PC2K cloud fractions against the co-located surface observations, separated by cloud class. Left: thin clouds; centre: medium optical thickness clouds; right: thick clouds. Bottom: Frequency histogram of the cloud fractions. Solid line: individual PC2K cloud fractions; dashed line: cloud fractions of co-located SYNOP observations. All data in August 1997, 1998 and 1999 are used.

ACPD
2, 623–668, 2002

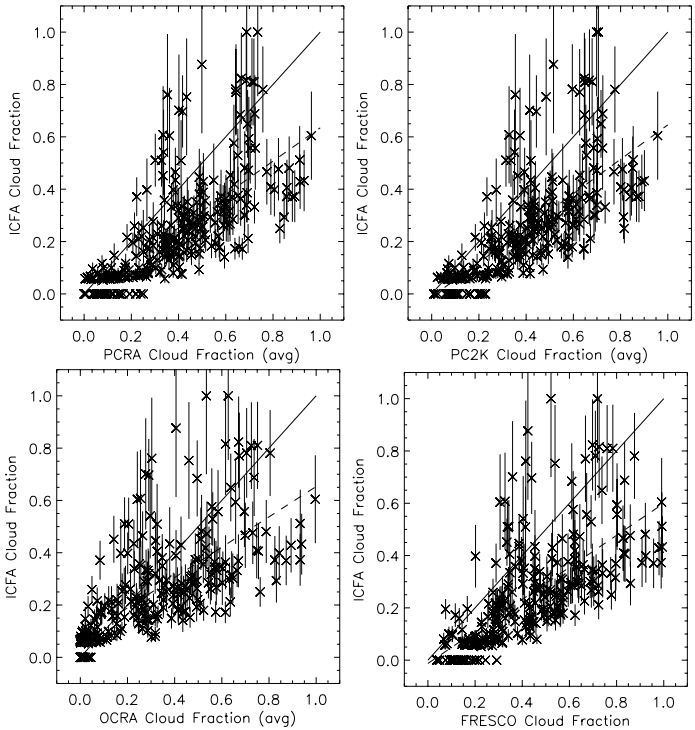

Fig. 7. A comparison of the cloud fraction averaged over all PMD sub-pixels in a GOME pixel against ICFA for the months of August 1997, 1998 and 1999. Top-left: PCRA, top-right: PC2K, bottom-left: OCRA, bottom-right: FRESCO. The dashed line is the linear regression through the points in the domain, the solid line indicates unity.

ACPD
2, 623–668, 2002

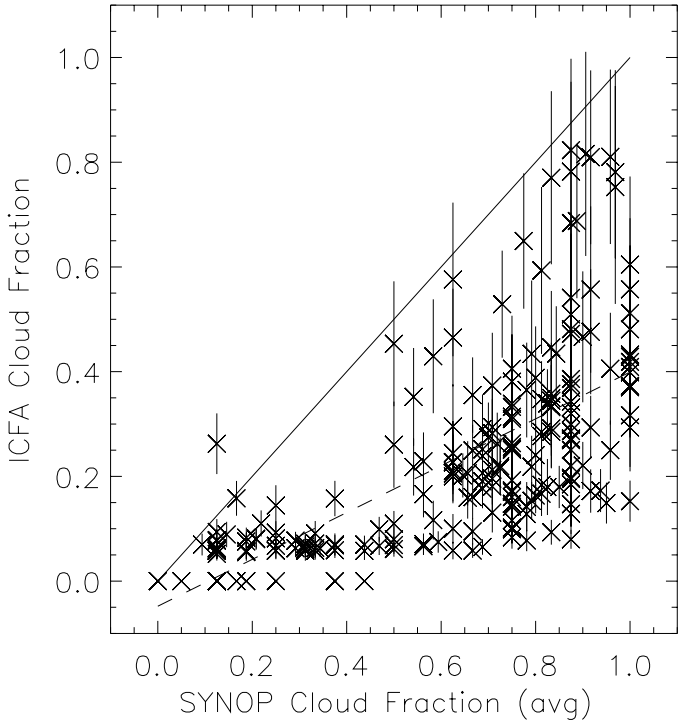

Fig. 8. A comparison between the cloud fraction from averaged co-located surface observations (SYNOP) against ICFA for August 1997, 1998 and 1999.

ACPD
2, 623–668, 2002

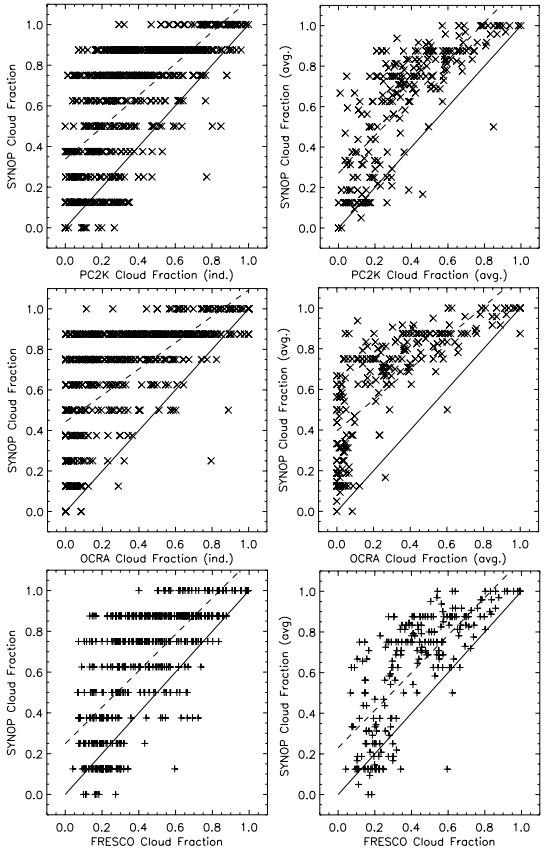

Fig. 9. A comparison between the cloud fractions of the individual PMD sub-pixels against individual co-located SYNOP surface observations (left) and averaged over a GOME pixel (right) for August 1997, 1998 and 1999 for PC2K (top) and OCRA (centre). Bottom: the FRESCO cloud fraction against individual SYNOP observations (left) and averaged (right).

ACPD
2, 623–668, 2002

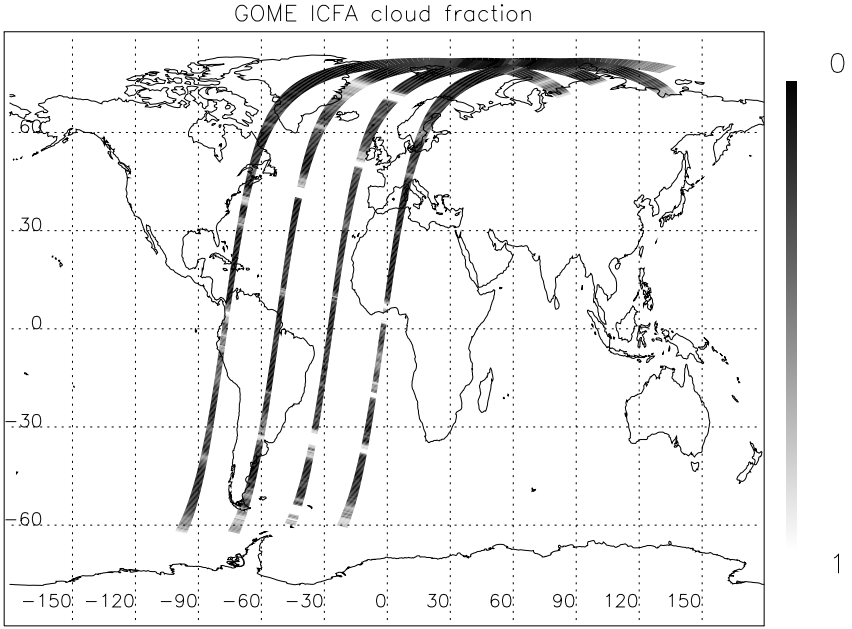

Fig. 10. ICFA cloud fractions along four GOME tracks in 2 August 1997. Only the centre (nadir) pixels are shown of tracks 70802101–70802151.

ACPD
2, 623–668, 2002

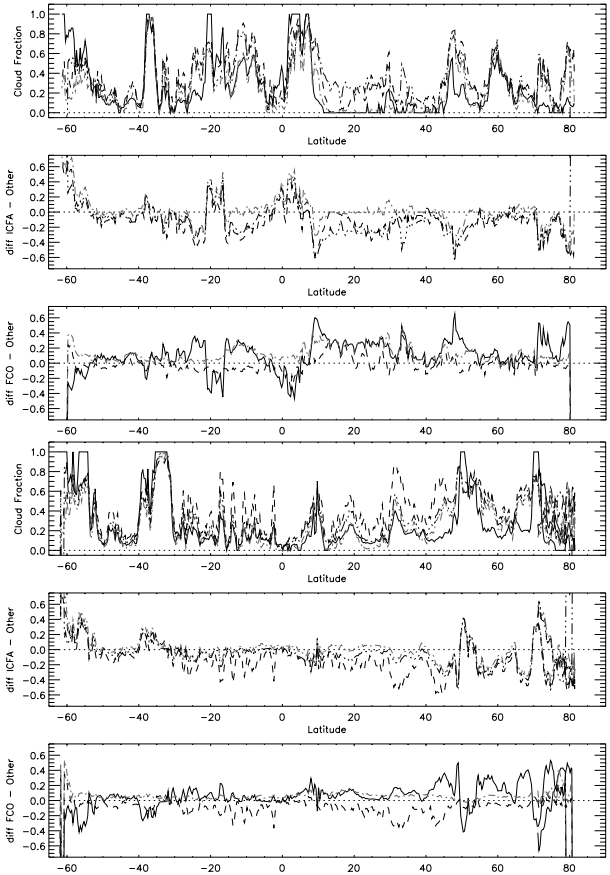

Fig. 11. Four GOME tracks on 2 August 1997. Centre pixels are shown. Top panel of each track: cloud fraction; middle panel: difference between ICFA and the other methods; bottom panel: difference between FRESCO and the other methods. Solid = ICFA, dashed = PCRA, light colored dashed = OCRA, dashdotdotdot = FRESCO. Tracks 70802101, 70802114, 70802132 and 70802151 are plotted.

ACPD
2, 623–668, 2002

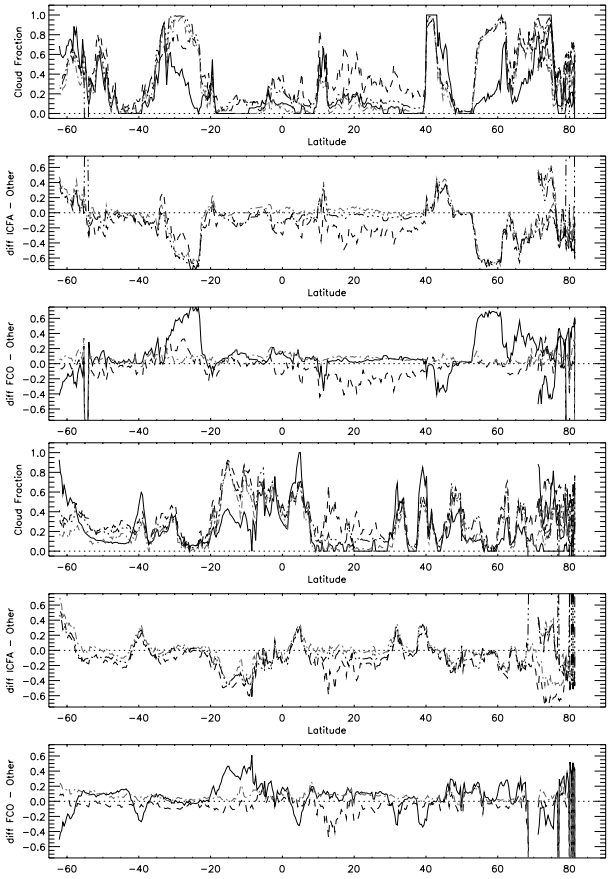

Fig. 11. Continued....

ACPD
2, 623–668, 2002